Interplay of ferromagnetism and spin-orbit coupling in $Sr_4Ru_3O_{10}$

Izidor Benedičič,[1,*] Masahiro Naritsuka,[1,*] Luke C. Rhodes,[1] Christopher Trainer,[1] Yoshiko Nanao,[1] Aaron B. Naden,[2] Rosalba Fittipaldi,[3] Veronica Granata,[4] Mariateresa Lettieri,[3] Antonio Vecchione,[3] and Peter Wahl[1,†]

[1] *School of Physics and Astronomy, University of St Andrews, North Haugh, St Andrews, Fife KY16 9SS, United Kingdom.*
[2] *School of Chemistry, University of St Andrews, North Haugh, St Andrews, Fife, KY16 9ST, United Kingdom*
[3] *CNR-SPIN, UOS Salerno, Via Giovanni Paolo II 132, Fisciano, I-84084, Italy.*
[4] *Dipartimento di Fisica "E. R. Caianiello", Università di Salerno, I-84084 Fisciano, Salerno, Italy.*

The ground state of metamagnetic materials can be controlled by magnetic field, promising new functionalities for spintronics applications. Yet, a microscopic understanding of the interplay of the electronic structure with the susceptibility to emergent orders is often missing, but would greatly facilitate optimization of the properties of metamagnetic materials. Here, we use low temperature scanning tunneling microscopy (STM) and spectroscopy to study the metamagnetism in the trilayer ruthenate $Sr_4Ru_3O_{10}$, combining STM-based magnetostriction measurements with quasiparticle-interference imaging (QPI) to elucidate the role of the microscopic electronic structure in the macroscopic metamagnetic properties. Our results highlight the importance of the orthorhombicity of the material for its metamagnetic properties, confirmed by magnetization measurements. Our QPI results show clear signatures of the minority spin bands crossing the Fermi energy, and provide a link between the ferromagnetic properties, spin-orbit coupling and the orthorhombicity of the crystal structure.

Controlling electronic properties through small stimuli is at the heart of modern electronics. Currently, gating is used to induce a linear response of a material to externally applied fields. Using correlation effects to boost the response promises potentially huge increases in efficiency, as significantly smaller stimuli may produce a comparable or even larger response. A class of materials that promises new opportunities for spintronics devices are metamagnetic materials, whose properties can be controlled through an applied magnetic field and which can be used, for example, for magnetic information storage.[1, 2] However, in many cases we do not have microscopic models for this behaviour, due to a lack of knowledge of the electronic structure in the relevant low energy regime – preventing tuning of these properties. QPI imaging has the energy resolution and capability to image the electronic structure as a function of magnetic field, promising understanding of macroscopic properties based on microscopic models.

The Ruddlesden-Popper series of the ruthenates with the chemical formula $Sr_{n+1}Ru_nO_{3n+1}$, where n is the number of RuO layers within a structural unit, host metamagnetic properties in several of their members. The triple layer compound, $Sr_4Ru_3O_{10}$ has an orthorhombic crystal structure with a unit cell of the space group *Pbam* with in-plane unit cell vectors $a = b = 3.9001$Å, and a unit cell height of $c = 28.573$Å.[3] It is a ferromagnet with a Curie temperature $T_C = 105\,K$.[3] Below T_C, the magnetic moment is oriented along the c-axis with evidence for canted magnetism[4, 5]. As the temperature is lowered, a metamagnetic transition occurs at $T_M = 50\,K$ [6]. Below T_M, a field-induced metamagnetic transition is found for an in-plane field of $\sim 2\,T$[6–8],

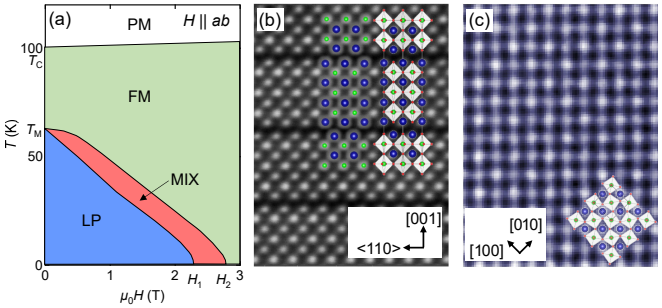

FIG. 1: (a) Schematic phase diagram of $Sr_4Ru_3O_{10}$ as a function magnetic field $\mu_0 H$ and temperature T with paramagnetic (PM), ferromagnetic (FM), lowly polarized (LP), and mixed (MIX) phases. (b) TEM image with the atomic structure superimposed (blue spheres: Sr, green spheres: Ru, red spheres: O). On the right, we show the atomic structure for one unit cell of $Sr_4Ru_3O_{10}$ with RuO_6 octahedra shown in grey. (c) Atomically resolved STM topography (10 nm × 10 nm, $T = 1.8\,K$). The surface is terminated by a Sr-O plane, showing the Sr square lattice. The crystal structure is shown as an overlay (colors as in b). Black arrows indicate the crystallographic axes [1 0 0] and [0 1 0] in the orthorhombic unit cell ($V = 30\,mV$, $I = 50\,pA$).

with evidence for a coexistence region in the phase diagram at the transition between the low-field phase and the high-field forced ferromagnetic phase (Fig. 1(a))[9]. Magnetoresistance suggests that in the forced ferromagnetic phase with the moments oriented in the plane, the Ru-O direction is the hard axis, with the easy axis at 45°[10].

Here, by a combination of QPI imaging using atomic-scale scanning tunneling spectroscopy with magnetiza-

tion and magnetostriction measurements in vector magnetic fields, we establish the role of spin-orbit coupling for the metamagnetic properties in $Sr_4Ru_3O_{10}$. Comparison of our QPI measurements with ab-initio calculations facilitates determination of the low energy electronic structure and shows that the electronic states at the Fermi energy are predominantly of spin minority character. In-situ bulk-sensitive magnetostriction measurements on the same sample allow us to directly relate the electronic structure to features of the bulk physical properties.

$Sr_4Ru_3O_{10}$ exhibits a natural cleavage plane between the SrO-layers on either side of the RuO trilayers, as can be seen in the cross-sectional TEM image in Fig. 1(b). Typical topographic STM images obtained at low temperatures (see section S1A of [11] for details) following sample cleavage and obtained at low temperatures show atomic resolution of the Sr lattice, Fig. 1(c), similar to what is observed on Sr_2RuO_4[12, 13] and $Sr_3Ru_2O_7$[14, 15].

To elucidate the role of the electronic structure of $Sr_4Ru_3O_{10}$ for the metamagnetic properties, we have measured QPI by recording spatial maps of the differential conductance $g(\mathbf{r}, V)$. Comparison with continuum LDOS (cLDOS) calculations based on a DFT-derived electronic structure with realistic modelling of the wave function overlap[11, 16–18] allows us to establish the low energy electronic structure. Fig. 2(a) shows the Fermi surface of $Sr_4Ru_3O_{10}$ obtained from a spin-polarized DFT calculation after inclusion of spin-orbit coupling. The Fermi surface is consistent with previous reports[19, 20]. It is dominated by bands of spin-minority character (Fig. S9(a) in [11]), with only a small hole-like pocket of spin-majority character crossing the Fermi energy at the Γ point. The exchange splitting obtained from the DFT calculation is approximately 1.1eV (Fig. S10 in [11]). Fig. 2(b, c) show the experimental QPI extracted from $g(\mathbf{r}, V)$-maps in comparison with the calculation. The most intense features arise from the large square-like Fermi surface sheets with minority spin character and exhibit excellent agreement between the calculations and experiment. The dispersion of this band, Fig. 2(c) and (d), is captured accurately once a band renormalization of 2.5 is accounted for. The dominant scattering vector appears split, which can be traced back to the double-square-like features in the Fermi surface with dominant d_{xz}/d_{yz}-character of the inner Fermi surface, and d_{xy}-character of the outer one. These QPI features show very little dependence on magnetic field, Fig. 2(d).

While the orthorhombicity of the crystal structure does not lead to clear C_4 symmetry breaking features in the QPI, it does result in an anisotropic field-dependence in spectroscopic maps. The most notable change in the momentum-dependent differential conductance, $g(\mathbf{q}, V)$, with in-plane fields occurs at the structural peaks, $\mathbf{q}_{\mathrm{at}} = (1, 0)$ and $(0, 1)$ (Fig. 3(a)). The energy-dependence of

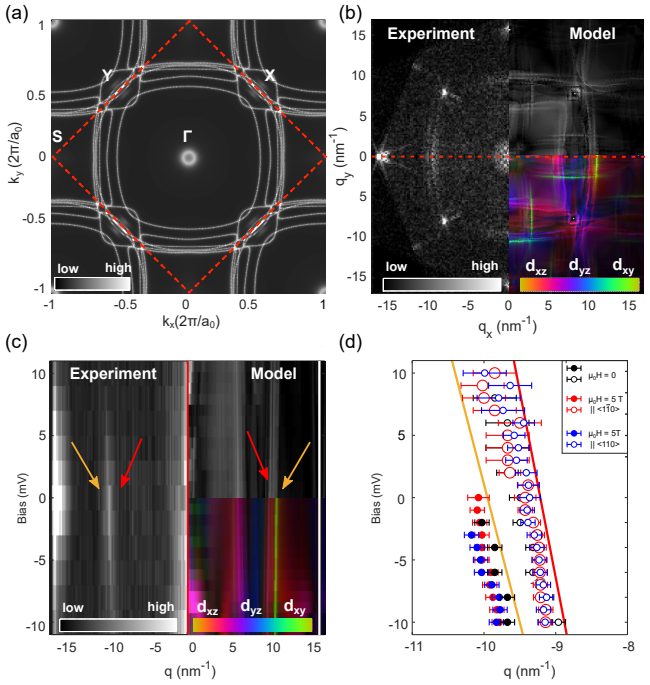

FIG. 2: (a) Fermi surface from a DFT-derived tight-binding model with magnetization along [0 0 1] [11]. The extended Brillouin zone corresponding to the Sr lattice is shown, dashed red square indicates the first Brillouin zone. (b) Left: Fourier transform of $g(\mathbf{r}, V)$ map for $V = -2$mV ($V_s = 30$mV, $I_s = 300$pA, $T = 1.8$K). Right: Simulated QPI at the Fermi energy. (c) Left: Cross-section of the map in (b) along the red dotted line. Two distinct bands are indicated by red and orange arrows. Right: Cross-section of the simulated QPI. (d) Dispersion in zero-field (black) and in-plane field along $\langle 1\,\bar{1}\,0\rangle$ and $\langle 1\,1\,0\rangle$. The main QPI signal exhibits a small splitting. The scattering signal with the smaller q-vector is visible at all energies, while the one with larger q disappears for $V > 0$mV consistent with the calculations in (c). Red and orange lines indicate calculated bands from (c).

the intensity of the structural peaks carries signatures of the van-Hove singularities.[13] Figs. 3b,c show line cuts through the atomic peaks for field along the [1 1 0] and [1 $\bar{1}$ 0] directions. We observe a shift in intensity $g(\mathbf{q}_{\mathrm{at}}, V)$ when the magnetic field is rotated from the [1 1 0] to the [1 $\bar{1}$ 0] direction, with the dominant intensity shifting from -2mV to 2mV. This behaviour is consistent with strong spin-orbit coupling. Due to the interplay of spin-orbit coupling, ferromagnetism and the orthorhombicity of the crystal structure, the band structure depends on the direction of the magnetization.[21, 22]. An in-plane magnetic field forces the magnetization into the direction of the field, resulting in changes of the electronic structure. The band structure in the vicinity of the Fermi energy shows changes close to the S point dependent on the magnetization direction (Fig. 3(d)). The spectral weight shift which we observe around the structural peaks is likely a consequence of these changes of the electronic struc-

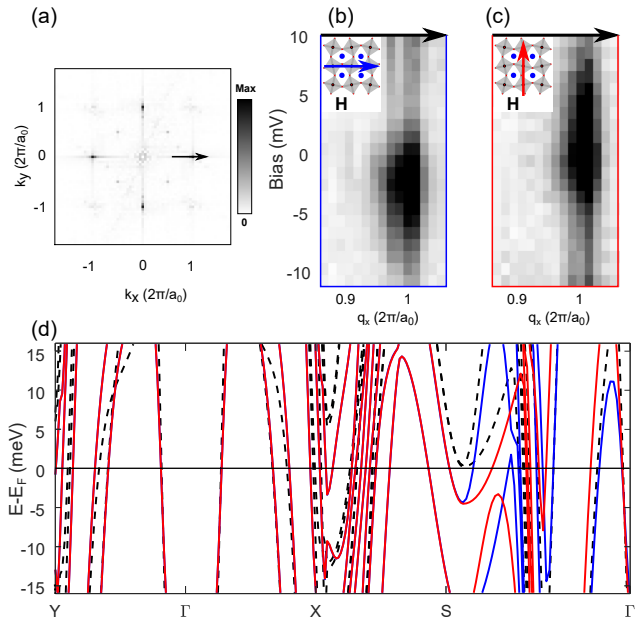

FIG. 3: (a) Fourier transform of topography. The black arrow indicates the direction of a cut across the atomic peak. (b), (c) cuts across the atomic peak at [1 1 0] from the experimental $g(\mathbf{q}, V)$ map for magnetic field $\mu_0\mathbf{H} = 5$T along [1 1 0] (b) and [1 $\bar{1}$ 0] (c). There is a clear shift of spectral weight dependent on the direction of **H**. (d) Band structure close to the Fermi energy including spin-orbit coupling with magnetization along [1 1 0] and [1 $\bar{1}$ 0], plotted in red and blue, respectively. Black dashed lines indicate the band structure without spin-orbit coupling.

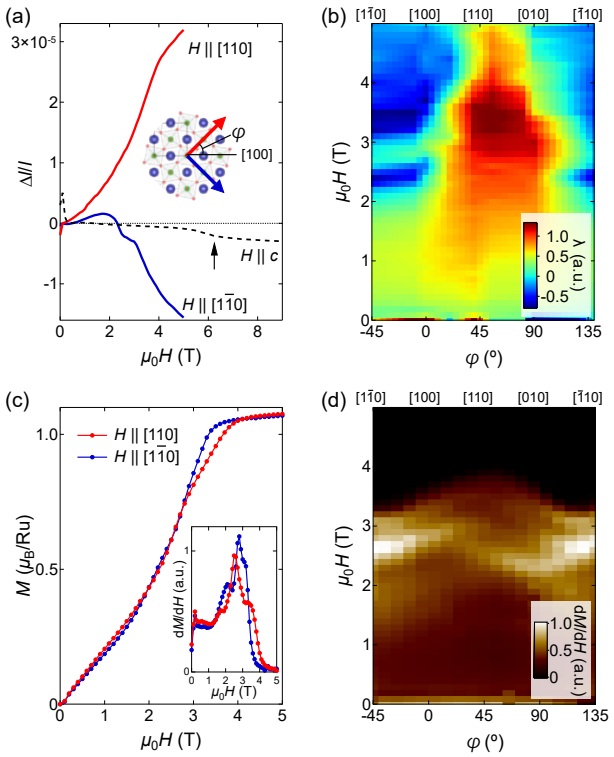

FIG. 4: (a) Field dependence of magnetostriction $\Delta l/l$ at $T = 1.8$ K. Black arrow indicates the metamagnetic transitions for $H \parallel [0\,0\,1]$. The inset shows directions of the field in the (0 0 1)-plane and definition of the angle φ. (b) Phase diagram as a function of field $\mu_0 H$ and φ showing the field derivative of the magnetostriction λ. A pronounced anisotropy can be seen between the [1 1 0] and [1 $\bar{1}$ 0] directions. (c) Isothermal magnetization as a function of $\mu_0 H$ at $T = 1.8$K for field in the (0 0 1)-plane. The inset shows dM/dH, showing clear differences between [1 1 0] (red) and [1 $\bar{1}$ 0] (blue). (d) Phase diagram in the $\mu_0 H$-φ plane showing the derivative of the magnetization with respect to field, $\mathrm{d}M/\mathrm{d}H$. See Fig. S2 in ref. 11 for the full angular dependence of the magnetic susceptibility.

ture. Not all experimental features match those of the model, as shown in Fig. S12(e), (f)[11]. We attribute the differences to the complexity of the band structure and because details on a millielectronvolt energy scale will sensitively depend on the magnitudes of exchange splitting, spin-orbit coupling strength and the renormalisations, which from the data presented here cannot be determined independently.

We see clear spectroscopic evidence that the electronic properties exhibit a reduced symmetry that follows the applied in-plane magnetic field, even though the structural anisotropy due to the orthorhombicity is tiny. We demonstrate in the following that this anisotropy is also reflected in the macroscopic physical properties of $Sr_4Ru_3O_{10}$. We use STM-based magnetostriction by measuring the field-dependence of the z-position of the STM tip while locking on a defect and ramping the field[23] on the same sample as used in the QPI measurements. This enables us to track the dimensions of the sample with sub-picometer resolution. Fig. 4(a) shows the normalized c-axis magnetostriction

$$\frac{\Delta l(\mu_0 H, 2\,\mathrm{K})}{l(0, 300\,\mathrm{K})} = \frac{l(\mu_0 H, 2\,\mathrm{K}) - l(0\,\mathrm{T}, 2\,\mathrm{K})}{l(0\,\mathrm{T}, 300\,\mathrm{K})} \qquad (1)$$

for magnetic fields $\mu_0\mathbf{H}$ along [0 0 1] as well as for the same in-plane directions, [1 1 0] and [1 $\bar{1}$ 0]. For field $\mu_0\mathbf{H} \parallel [0\,0\,1]$, a kink at $\sim$ 6T is observed, indicated by a black arrow in Fig. 4(a). For fields $\mu_0\mathbf{H}$ in the (0 0 1) plane, we find a more complex behavior, Fig. 4(a, b): For $\mu_0\mathbf{H} \parallel [1\,\bar{1}\,0]$, the magnetostriction shows a two-hump behavior (blue curve in Fig. 4(a)). The first maximum is at $\sim$ 2.4T and the second at $\sim$ 3.2T. For $\mu_0\mathbf{H} \parallel [1\,1\,0]$ (red curve in Fig. 4(a)), the magnetostriction exhibits a radically different behaviour, showing a monotonous increase with a kink at $\sim$ 3.5T and no minimum. This two-fold symmetric behavior is confirmed by the detailed dependence of the magnetostriction on the angle φ. In Fig. 4(b), we plot the $H - \varphi$ dependence of the linear magnetostriction coefficient $\lambda = \frac{\partial}{\partial H}\frac{\Delta l}{l}$. The significant in-plane anisotropy is confirmed in magnetization in vector magnetic fields, Fig. 4(c, d). Measurements of the magnetization as a function of field $\mu_0 H$

for $\mathbf{H} \parallel [1\,1\,0]$ or $[1\,\bar{1}\,0]$ confirm significant differences: the field at which the magnetization saturates is significantly higher for field along $[1\,1\,0]$ compared to field along $[1\,\bar{1}\,0]$ (Fig. 4(c)). Fig. 4(d) shows the detailed angular dependence of the magnetization. For a tetragonal crystal structure, one would expect a four-fold symmetry of the angular dependence, however we again see a clear two-fold symmetry.

Our results demonstrate the interplay between magnetism, spin-orbit coupling and orthorhombicity for the metamagnetic properties of $Sr_4Ru_3O_{10}$. While the difference in lattice constants between the a and b directions is only about 0.04%, it leaves clearly measurable traces in the response to magnetic field. Our QPI measurements allow us to link the physical properties to characteristics of the electronic structure. From the comparison of the calculated and measured QPI, we can determine the low energy electronic structure. The Fermi surface obtained from QPI is dominated by bands with minority spin character and in close agreement with previous ARPES measurements [20]. A good description of the QPI is obtained with a renormalization of the DFT band structure by ~ 2.5. We can estimate from our model an electronic contribution to the specific heat of $31\frac{\mathrm{mJ}}{\mathrm{mol(Ru)K^2}}$, close to the experimental value of $(19 \pm 4)\frac{\mathrm{mJ}}{\mathrm{mol(Ru)K^2}}$ [24].

In STM-based dilatometric measurements, we observe a double metamagnetic transition through a two-fold hump feature similar to what has been reported in recent magnetization measurements[7]. The origin of this feature has been suggested to be either due to magnetic order in two inequivalent Ru sites in the trilayered $Sr_4Ru_3O_{10}$ or the splitting of van Hove singularities due to interactions between adjacent layers within a trilayer [7]. The most notable result of our measurements is the significant difference between the response to field along the crystallographic $[1\,1\,0]$ and $[1\,\bar{1}\,0]$ directions. The observed non-monotonic behaviour and the field at which the transition occurs is consistent with previous dilatometric measurements [25], whereas a previous study of the unit cell parameters as a function of field by neutron scattering[26] shows the transition in the c-axis lattice constant at a lower in-plane field compared to magnetostriction. One possible origin for this difference may be the precise in-plane direction of the field, which is not known in the neutron scattering experiment.

Our results uncover the importance of orthorhombicity for the metamagnetism in $Sr_4Ru_3O_{10}$, despite the tiny anisotropy in the lattice constants. Through realistic modelling of the quasiparticle interference, we can determine the electronic structure in the vicinity of the Fermi energy. We show that spin-orbit coupling leads to an anisotropic response of the electronic structure to in-plane magnetic fields.

ACKNOWLEDGMENTS

We gratefully acknowledge useful discussions with P. Ngabonziza, as well as Stephen L. Lee and Andreas W. Rost who setup the MPMS facility enabling the vector field measurements. IB acknowledges funding through the International Max Planck Research School for Chemistry and Physics of Quantum Materials, MN, CT and PW through EP/R031924/1 and EP/T031441/1 and LCR from the Royal Commission of the Exhibition of 1851. TEM measurements were supported through grants EP/R023751/1, EP/L017008/1 and EP/T019298/1. YN acknowledges support through the ERC grant ERC-714193-QUESTDO held by Phil King.

* These authors contributed equally.
† Correspondence to: wahl@st-andrews.ac.uk.

[1] X. Marti, I. Fina, C. Frontera, J. Liu, P. Wadley, Q. He, R. J. Paull, J. D. Clarkson, J. Kudrnovský, I. Turek, J. Kuneš, D. Yi, J.-H. Chu, C. T. Nelson, L. You, E. Arenholz, S. Salahuddin, J. Fontcuberta, T. Jungwirth, and R. Ramesh, Nature Mater **13**, 367 (2014).
[2] T. Moriyama, N. Matsuzaki, K.-J. Kim, I. Suzuki, T. Taniyama, and T. Ono, Appl. Phys. Lett. **107**, 122403 (2015).
[3] M. K. Crawford, R. L. Harlow, W. Marshall, Z. Li, G. Cao, R. L. Lindstrom, Q. Huang, and J. W. Lynn, Phys. Rev. B **65**, 214412 (2002).
[4] R. Gupta, M. Kim, H. Barath, S. L. Cooper, and G. Cao, Phys. Rev. Lett. **96**, 067004 (2006).
[5] H. Zheng, W. H. Song, J. Terzic, H. D. Zhao, Y. Zhang, Y. F. Ni, L. E. DeLong, P. Schlottmann, and G. Cao, Phys. Rev. B **98**, 064418 (2018).
[6] G. Cao, L. Balicas, W. H. Song, Y. P. Sun, Y. Xin, V. A. Bondarenko, J. W. Brill, S. Parkin, and X. N. Lin, Phys. Rev. B **68**, 174409 (2003).
[7] E. Carleschi, B. P. Doyle, R. Fittipaldi, V. Granata, A. M. Strydom, M. Cuoco, and A. Vecchione, Phys. Rev. B **90**, 205120 (2014).
[8] Y. J. Jo, L. Balicas, N. Kikugawa, E. S. Choi, K. Storr, M. Zhou, and Z. Q. Mao, Phys. Rev. B **75**, 094413 (2007).
[9] D. Fobes, M. H. Yu, M. Zhou, J. Hooper, C. J. O'Connor, M. Rosario, and Z. Q. Mao, Phys. Rev. B **75**, 094429 (2007).
[10] D. Fobes, T. J. Liu, Z. Qu, M. Zhou, J. Hooper, M. Salamon, and Z. Q. Mao, Phys. Rev. B **81**, 172402 (2010).
[11] "Supplementary material," (2022).
[12] Z. Wang, D. Walkup, P. Derry, T. Scaffidi, M. Rak, S. Vig, A. Kogar, I. Zeljkovic, A. Husain, L. H. Santos, Y. Wang, A. Damascelli, Y. Maeno, P. Abbamonte, E. Fradkin, and V. Madhavan, Nature Physics **13**, 799 (2017).
[13] C. A. Marques, L. C. Rhodes, R. Fittipaldi, V. Granata, C. M. Yim, R. Buzio, A. Gerbi, A. Vecchione, A. W. Rost, and P. Wahl, Advanced Materials **33**, 2100593 (2021).

[14] K. Iwaya, S. Satow, T. Hanaguri, N. Shannon, Y. Yoshida, S. I. Ikeda, J. P. He, Y. Kaneko, Y. Tokura, T. Yamada, and H. Takagi, Phys. Rev. Lett. **99**, 057208 (2007).
[15] C. A. Marques, L. C. Rhodes, I. Benedičič, M. Naritsuka, A. B. Naden, Z. Li, A. C. Komarek, A. P. Mackenzie, and P. Wahl, arXiv:2202.12351 [cond-mat] (2022).
[16] A. Kreisel, P. Choubey, T. Berlijn, W. Ku, B. Andersen, and P. Hirschfeld, Phys. Rev. Lett. **114**, 217002 (2015).
[17] A. Kreisel, R. Nelson, T. Berlijn, W. Ku, R. Aluru, S. Chi, H. Zhou, U. R. Singh, P. Wahl, R. Liang, W. N. Hardy, D. A. Bonn, P. J. Hirschfeld, and B. M. Andersen, Phys. Rev. B **94**, 224518 (2016).
[18] A. Kreisel, C. A. Marques, L. C. Rhodes, X. Kong, T. Berlijn, R. Fittipaldi, V. Granata, A. Vecchione, P. Wahl, and P. J. Hirschfeld, npj Quantum Mater. **6**, 100 (2021).
[19] G. Gebreyesus, P. Ngabonziza, J. Nagura, N. Seriani, O. Akin-Ojo, and R. M. Martin, Phys. Rev. B **105**, 165119 (2022).
[20] P. Ngabonziza, E. Carleschi, V. Zabolotnyy, A. Taleb-Ibrahimi, F. Bertran, R. Fittipaldi, V. Granata, M. Cuoco, A. Vecchione, and B. P. Doyle, Sci Rep **10**, 21062 (2020).
[21] S. Raghu, A. Paramekanti, E. A. Kim, R. A. Borzi, S. A. Grigera, A. P. Mackenzie, and S. A. Kivelson, Phys. Rev. B **79**, 214402 (2009).
[22] C. M. Puetter, J. G. Rau, and H.-Y. Kee, Phys. Rev. B **81**, 081105 (2010).
[23] C. Trainer, C. Abel, S. L. Bud'ko, P. C. Canfield, and P. Wahl, Phys. Rev. B **104**, 205134 (2021).
[24] X. Lin, V. Bondarenko, G. Cao, and J. Brill, Solid State Communications **130**, 151 (2004).
[25] W. Schottenhamel, M. Abdel-Hafiez, R. Fittipaldi, V. Granata, A. Vecchione, M. Hücker, A. U. B. Wolter, and B. Büchner, Phys. Rev. B **94**, 155154 (2016).
[26] V. Granata, L. Capogna, M. Reehuis, R. Fittipaldi, B. Ouladdiaf, S. Pace, M. Cuoco, and A. Vecchione, J. Phys.: Condens. Matter **25**, 056004 (2013).
[27] C. Trainer, C. M. Yim, M. McLaren, and P. Wahl, Review of Scientific Instruments **88**, 093705 (2017).
[28] R. Fittipaldi, D. Sisti, A. Vecchione, and S. Pace, Crystal Growth & Design **7**, 2495 (2007).
[29] P. Giannozzi, S. Baroni, N. Bonini, M. Calandra, R. Car, C. Cavazzoni, Davide Ceresoli, G. L. Chiarotti, M. Cococcioni, I. Dabo, A. D. Corso, S. d. Gironcoli, S. Fabris, G. Fratesi, R. Gebauer, U. Gerstmann, C. Gougoussis, Anton Kokalj, M. Lazzeri, L. Martin-Samos, N. Marzari, F. Mauri, R. Mazzarello, Stefano Paolini, A. Pasquarello, L. Paulatto, C. Sbraccia, S. Scandolo, G. Sclauzero, A. P. Seitsonen, A. Smogunov, P. Umari, and R. M. Wentzcovitch, J. Phys.: Condens. Matter **21**, 395502 (2009).
[30] J. P. Perdew, K. Burke, and M. Ernzerhof, Phys. Rev. Lett. **77**, 3865 (1996).
[31] A. A. Mostofi, J. R. Yates, G. Pizzi, Y.-S. Lee, I. Souza, D. Vanderbilt, and N. Marzari, Computer Physics Communications **185**, 2309 (2014).
[32] M. W. Haverkort, I. S. Elfimov, L. H. Tjeng, G. A. Sawatzky, and A. Damascelli, Phys. Rev. Lett. **101**, 026406 (2008).
[33] T. Scaffidi, J. C. Romers, and S. H. Simon, Phys. Rev. B **89**, 220510 (2014).
[34] A. Tamai, M. Zingl, E. Rozbicki, E. Cappelli, S. Riccò, A. de la Torre, S. McKeown Walker, F. Bruno, P. King, W. Meevasana, M. Shi, M. Radović, N. Plumb, A. Gibbs, A. Mackenzie, C. Berthod, H. Strand, M. Kim, A. Georges, and F. Baumberger, Phys. Rev. X **9**, 021048 (2019).
[35] P. Choubey, T. Berlijn, A. Kreisel, C. Cao, and P. J. Hirschfeld, Phys. Rev. B **90**, 134520 (2014).